

Strategy of Topology Selection Based on Quasi-Duality Between Series–Series and Series–Parallel Topologies of Resonant Inductive Coupling Wireless Power Transfer Systems

Masataka Ishihara , *Student Member, IEEE*, Kazuhiro Umetani , *Member, IEEE*, and Eiji Hiraki, *Member, IEEE*

Abstract—Series–series (SS) and series–parallel (SP) topologies are widely used in resonant inductive coupling wireless power transfer systems for various applications. However, the selection of an appropriate topology to achieve higher output power or higher efficiency is typically difficult because design optimization of the circuit parameters (e.g., characteristic impedance, load resistance, and mutual inductance) for each topology is generally separately discussed using different equivalent circuits with multiple resonance modes. Therefore, the purpose of this study involves proposing a simple strategy to select an appropriate topology. The proposed strategy is based on quasi-duality between the SS and SP topologies that are elucidated from the novel equivalent circuits derived using Lagrangian dynamics. Based on the quasi-duality, the output power and efficiency of the SP topology are calculated via the equivalent circuit of SS topology. Thus, the quasi-duality offers a simple comparison between the SS and SP topologies. The proposed strategy selects an appropriate topology by comparing only the equivalent ac load resistance, which is the ac resistance including the rectifying circuit and the load resistance, the characteristic impedance, and the ac load resistance that achieves the maximum efficiency or maximum output power of the SS topology. Experiments verify the appropriateness and effectiveness of the proposed strategy.

Index Terms—Circuit topology, efficiency, equivalent circuit, inductive power transmission, lagrangian dynamics, output power, series–parallel topology, series–series topology, wireless power transmission.

I. INTRODUCTION

WIRELESS power transfer (WPT) techniques are attracting significant attention as an emerging technology for power supplies. The WPT techniques can overcome the need for physical cable connections. Thus, the WPT techniques realize convenient, reliable, and safe power supplies. Specifically, resonant inductive coupling WPT (RIC-WPT) systems via the

Manuscript received April 18, 2019; revised August 25, 2019; accepted October 31, 2019. Date of publication November 27, 2019; date of current version March 13, 2020. This article was presented in part at the International Conference on Power Electronics and Drive Systems, Honolulu, HI, USA, December 2017 [9]. Recommended for publication by Associate Editor J. Itoh. (Corresponding author: Masataka Ishihara.)

The authors are with the Graduate School of Natural Science and Technology, Okayama University, Okayama 700-8530, Japan (e-mail: p4wv0vf6@okayama-u.ac.jp; umetani@okayama-u.ac.jp; hiraki@okayama-u.ac.jp).

Color versions of one or more of the figures in this article are available online at <http://ieeexplore.ieee.org>.

Digital Object Identifier 10.1109/TPEL.2019.2956732

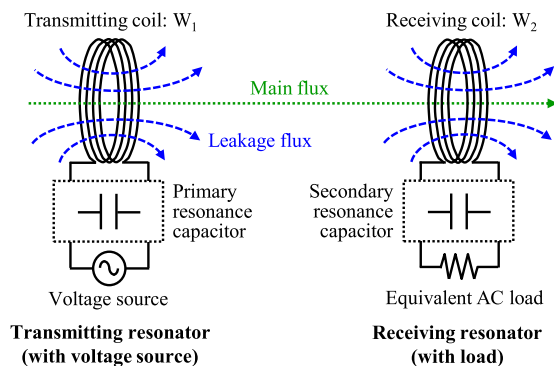


Fig. 1. Typical resonant inductive coupling wireless power transfer system.

magnetic induction between loosely coupled coils are widely studied as a high-efficiency WPT technique for various applications including electric vehicles [1]–[3], mobile devices [4], and biomedical devices [5], [6].

Fig. 1 illustrates the typical RIC-WPT system where W_1 and W_2 denote the transmitting and receiving coils, respectively. As shown in Fig. 1, significant leakage flux is generated because magnetic coupling between the coils is typically significantly weak. Reactive impedance due to the leakage flux decreases the power factor and output power. Therefore, in the RIC-WPT systems, the resonance capacitor is connected to each coil to cancel the reactive impedance [2], [3], [7]–[13].

The RIC-WPT systems are mainly classified into two basic topologies known as series–series (SS) and series–parallel (SP) topologies based on the connection of the secondary resonance capacitor [1]–[16]. Between the SS and SP topologies, an appropriate topology must be selected based on specifications for various applications at the beginning of the RIC-WPT design. The output power at a given voltage of the source [2], [7] and efficiency [13], [14] are typically considered as the performance criteria to select an appropriate topology.

However, the selection of an appropriate topology is typically difficult when comparing the output power and the efficiency between the SS and SP topologies. The SS and SP topologies are analyzed and designed separately based on different equivalent circuits with multiple resonant modes due to the frequency splitting phenomenon [2], [5], [6], [10], [12], [17], [18]. The

complicated operating principle due to the multiple resonant modes prevents a straightforward comparison of the circuit performances based on the values of the circuit parameter such as characteristic impedance, equivalent ac load resistance, which is the ac resistance including the rectifying circuit and the load resistance, and mutual inductance.

Strategies to select an appropriate topology between the SS and SP topologies are discussed in a few previous studies [13], [14]. Extant studies, including [13] and [14], investigated which SS and SP topologies achieve higher efficiency based on a value of the operating frequency [13] or the equivalent ac load resistance [14]. The strategies are simple, and effectiveness was successfully confirmed in the aforementioned studies. However, the discussions in [13] and [14] are limited to a basic case wherein the operating frequency is equal to the natural resonance frequencies of the transmitting resonator (transmitter) and receiving resonator (receiver). Thus, the strategy of the topology selection is not clear at different frequencies from the natural resonance frequency of the resonators that includes frequencies corresponding to the multiple resonant modes. Additionally, the strategy of the topology selection in terms of the output power is still unknown. Establishing the strategy of topology selection in terms of the output power is more difficult than in terms of efficiency because the output power is easily affected by the frequency splitting phenomenon.

Certainly, [19] compared the SS and SP topologies at some more operating frequencies other than the natural resonance frequency. However, this study also specified the operating frequency for comparison. Therefore, the operating frequency for comparison is still limited in these extant studies. The reason for this limitation may lie in the fact that these extant studies analyzed the SS and SP topologies using the circuit theory. According to the circuit theory, the SS and SP topologies have different circuit configurations, which make the comparison difficult over a continuous operating frequency range near the natural resonance frequency.

A key to establishing a straightforward strategy for the topology selection may correspond to the duality relation between the SS and SP topologies. The duality [20], [21] is well known as a promising concept for the derivation of novel circuits [22] and the analysis of circuit behavior [9], [23], [24]. Two circuits under the duality relation exhibit the same behavior in terms of the input/output power. Conversely, the current and voltage of circuit elements are interchanged. Hence, the circuits under the duality relation follow the same circuit equations with the exception that the role of the voltage and current are interchanged. Therefore, the performance of the circuits under the duality relation is analyzed via the same equivalent circuit. Hence, if the duality relation between the SS and SP topologies can be elucidated, then the analysis result of either topology may be shared with the other topology. This can result in a straightforward comparison of the output power and efficiency based on the change of various circuit parameters. Furthermore, sharing the same equivalent circuit will lead to avoiding the problem of the extant studies for comparing the SS and SP topologies. Consequently, the duality relation can result in a simple but generalized topology selection strategy that is not limited to some specific frequencies but can

be applicable over a continuous operating frequency range near the natural resonance frequency.

Recently, the duality relation between the SS and SP topologies was elucidated via analyzing novel equivalent circuits derived using Lagrangian dynamics [9]. Based on [9], the SP topology approximately works as the dual of the SS topology in which the equivalent ac load resistance R is replaced by Z^2/R where Z denotes the characteristic impedance of the receiver. An extant study by [9] referred to the relation as quasi-duality because it is close to duality. This knowledge is promising because the output power and efficiency of the SP topology are calculated using the equivalent circuit of SS topology in which the equivalent ac load resistance is transformed. Thus, the selection of an appropriate topology is reduced to determining which R and Z^2/R are preferable in the equivalent circuit of SS topology.

However, the selection of an appropriate topology discussed in [9] continues to be complicated. In order to select an appropriate topology, it is necessary to calculate and compare output power and the efficiency at the two types of equivalent ac load resistances corresponding to each topology by using the equivalent circuit of SS topology. This procedure is potentially tedious and time consuming. If simple boundaries for the performances (i.e., the output power and efficiency) between the SS and SP topologies are elucidated using quasi-duality, a more simple and general strategy for topology selection can be obtained.

Therefore, the purpose of this article is to propose a straightforward topology selection strategy from the SS and SP topologies. The proposed strategy can choose the preferable topology with greater output power and better efficiency by only comparing the three resistances explicitly defined using the circuit parameters. The derivation of the strategy is based on the quasi-duality relation between the SS and SP topologies, which was elucidated in [9] using the Lagrangian dynamics. Along with the review of [9], i.e., the quasi-duality relation, this article presents the analysis of the quasi-duality relation, which is newly performed to derive the proposed strategy. The derivation of this strategy is the additional content from [9].

The proposed strategy is only applicable to the topology selection between the SS and SP topologies, although a number of other topologies have been proposed in the literature [25]. Therefore, the practical application of the proposed strategy may still be limited. However, the derivation of the topology selection strategy is based on the quasi-duality relation, which has been recently elucidated by [9] using the Lagrangian dynamics. The Lagrangian dynamics is a recently developed analysis technique [21], [24], [26]–[30]; and therefore, the application know-how of this technique is still under development. Currently, Lagrangian dynamics succeeded to derive the quasi-duality relation between the SS and SP topologies. However, this technique can be expected to elucidate the similar relations among various topologies in the near future. Then, the topology selection strategy can also be expected to be derived for various topologies based on a similar analysis method as that presented in this article.

The study is organized into the following four sections. Section II reviews the quasi-duality between the SS and SP topologies based on [9]. Section III proposes a strategy for topology selection based on quasi-duality. Section IV verifies

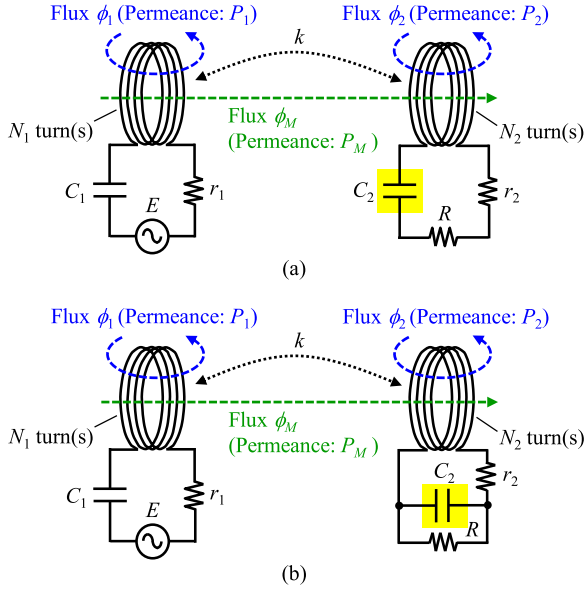


Fig. 2. Circuit models of RIC-WPT system. (a) SS topology. (b) SP topology.

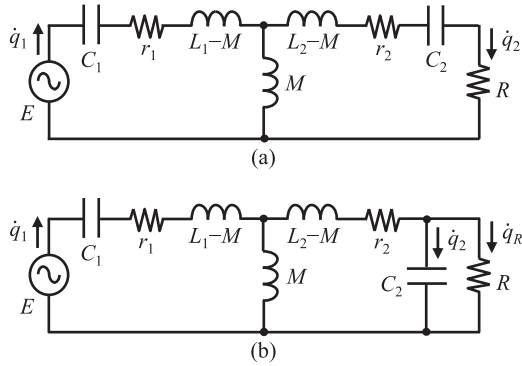


Fig. 3. Original T-shaped equivalent circuit. (a) SS topology. (b) SP topology.

the appropriateness and effectiveness of the proposed strategy via experiments and simulations. Finally, Section V concludes the study.

II. QUASI-DUALITY BETWEEN SS AND SP TOPOLOGIES

A. Procedure for Elucidation of Quasi-Duality

First, this subsection shows the procedure to elucidate the quasi-duality between the SS and SP topologies. Fig. 2 shows the circuit model of the SS and SP topologies of the RIC-WPT. Symbol E denotes the voltage of voltage source; R denotes the equivalent ac load resistance; N_1 and N_2 denote the number of turns of the transmitting coil (W_1) and the receiving coil (W_2); r_1 and r_2 denote the parasitic resistance of W_1 and W_2 ; P_1 , P_2 , and P_M denote the permeance of the flux ϕ_1 , ϕ_2 , and ϕ_M , respectively; k denotes the coupling coefficient between W_1 and W_2 ; and C_1 and C_2 denote the capacitance. Fig. 3 illustrates the equivalent circuits of Fig. 2 in which the loosely coupled coils are replaced with the T-shaped equivalent circuit. Symbol L_1 and L_2 denote the self-inductance of W_1 and W_2 ; M denotes the mutual

inductance; and q_1 , q_2 , and q_R denote the time integration of the current, and a dot over a variable indicates its time derivative. Additionally, L_1 , L_2 , and M are defined as follows:

$$L_1 = L_{leak1} + \frac{N_1}{N_2} M$$

$$L_2 = L_{leak2} + \frac{N_2}{N_1} M$$

$$M = k\sqrt{L_1 L_2} = N_1 N_2 P_M$$

$$L_{leak1} = N_1^2 P_1$$

$$L_{leak2} = N_2^2 P_2 \quad (1)$$

where L_{leak1} and L_{leak2} denote the leakage inductance of the transmitting and receiving sides, respectively.

Any duality between the SS and SP topologies is absent as shown in Figs. 2 and 3. However, quasi-duality is elucidated by analyzing the equivalent circuits based on the following five steps [9].

- 1) The novel equivalent circuit of SS topology is derived by applying Lagrangian dynamics [26] to the original equivalent circuit, i.e., Fig. 2(a).
- 2) As in step 1, the original equivalent circuit of SP topology, i.e., Fig. 2(b), is transformed via Lagrangian dynamics.
- 3) The duality transformation is applied to the equivalent circuit of the SP topology obtained in step 2.
- 4) Furthermore, the Δ -Y transformation, Thevenin's theorem, an impedance transformation, and practical approximations are applied to the dual circuit of the SP topology obtained in step 3.
- 5) Finally, the dual circuit of SP topology obtained in step 4 is compared with the equivalent circuit of SS topology obtained in step 1.

B. Lagrangian Equivalent Circuit of SS Topology (Step 1)

Recently, the Lagrangian modeling method originally proposed in [26] was demonstrated to be effective for power electronics researches. Lagrangian dynamics can derive various equivalent circuits that can scarcely be derived using circuit theory. Thus, Lagrangian dynamics offers novel insights (e.g., the quasi-duality between the SS and SP topologies of the RIC-WPT) that are not obtained using only circuit theory. Other applications of Lagrangian dynamics include the derivation of simple analysis models for integrated magnetic components [27], [28], duality transformation method for nonplanar circuits [21], elucidation of the quasi-duality between the SS and SP topologies of the resonant capacitive coupling WPT systems [24], derivation of a novel simple equivalent circuit of the RIC-WPT system with dual transmitting resonators [29], and Lagrangian-based development of a sliding-mode control for the synchronous converter [30].

The derivation method of a novel equivalent circuit using Lagrangian dynamics consists of the following three systematic procedures. First, the Lagrangian and dissipation function, i.e., the Lagrangian model, of the conventional circuit model is configured. Second, an appropriate coordinate transformation is

applied to the Lagrangian model obtained via the first procedure. The coordinate transformation conserves the circuit behavior for power. Thus, another Lagrangian model belonging to a different circuit topology is obtained in the procedure. Third, the Lagrangian model obtained in the second procedure is translated into a circuit diagram. In this study, the equivalent circuit obtained using Lagrangian dynamics is termed as the Lagrangian equivalent circuit.

Based on [9] and [26], we construct the Lagrangian model of SS topology shown in Fig. 3(a). For the purpose of convenience, all the capacitors are assumed to not exhibit an initial charge. The Lagrangian Λ_{SS} and dissipation function D_{SS} are formulated as follows:

$$\begin{aligned} \Lambda_{SS} = & N_1 \dot{q}_1 (\phi_1 + \phi_M) + N_2 \dot{q}_2 (\phi_2 - \phi_M) - \phi_1^2/2P_1 \\ & - \phi_2^2/2P_2 - \phi_M^2/2P_M - q_1^2/2C_1 - q_2^2/2C_2 + Eq_1 \end{aligned} \quad (2)$$

$$D_{SS} = R\dot{q}_2^2/2 + r_1\dot{q}_1^2/2 + r_2\dot{q}_2^2/2. \quad (3)$$

In the right-hand side of (2), the first to fifth terms denote the Lagrangian of W_1 and W_2 ; the sixth and seventh terms denote the Lagrangian of the capacitors; and the eighth term denotes the Lagrangian of the voltage source. Furthermore, in the right-hand side of (3), the first term denotes the dissipation function of the equivalent ac load resistance, and the second and third terms denote the dissipation function of the parasitic resistance.

Subsequently, an appropriate coordinate transformation is applied to (2) and (3) to yield another Lagrangian model that belongs to another circuit model. Thus, new variables q_A , q_B , ϕ_A , and ϕ_B are introduced as follows:

$$\begin{aligned} q_A &= \frac{\alpha (N_2 C_2 q_1 + N_1 C_1 q_2)}{2N_1 C_1} \\ q_B &= \frac{\beta (N_1 q_1 - N_2 q_2)}{2N_2} \\ \phi_A &= P_1 (\phi_1 + \phi_2)/(P_1 + P_2) \\ \phi_B &= (P_2 \phi_1 - P_1 \phi_2)/(P_1 + P_2) \end{aligned} \quad (4)$$

where the dimensionless quantity of α and β are defined as follows:

$$\begin{aligned} \alpha &= \frac{2N_1^2 C_1}{N_1^2 C_1 + N_2^2 C_2} \\ \beta &= \frac{2N_2^2 C_2}{N_1^2 C_1 + N_2^2 C_2}. \end{aligned} \quad (5)$$

We substitute (4) into (2) and (3) to obtain the following expressions:

$$\begin{aligned} \Lambda_{SS} = & 2N_2 (\dot{q}_A \phi_A + \dot{q}_B \phi_B + \dot{q}_B \phi_M) / \beta - q_A^2 / \alpha C_1 \\ & - q_B^2 / \beta C_2 - \phi_A^2 / \beta P_1 - \phi_B^2 / \beta P_2 - \phi_M^2 / 2P_M \\ & + Eq_A N_2 / N_1 + Eq_B N_1 C_1 / N_2 C_2 \end{aligned} \quad (6)$$

$$\begin{aligned} D_{SS} = & R(\dot{q}_A - \dot{q}_B)^2/2 + C_1 r_1 / C_2 (\dot{q}_A / \alpha + \dot{q}_B / \beta) \\ & + (C_2 r_2 - C_1 r_1) (\dot{q}_A - \dot{q}_B)^2 / 2C_2. \end{aligned} \quad (7)$$

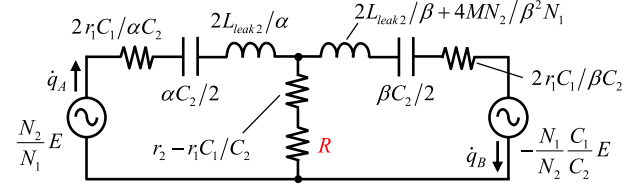


Fig. 4. Lagrangian equivalent circuit of SS topology.

In order to derive (6) and (7), we introduce the practical approximation, i.e., $L_{leak1} C_1 \approx L_{leak2} C_2$. We assume that the resonance frequencies of the transmitter and receiver are equal as is natural for a common design of the RIC-WPT systems. Furthermore, in the RIC-WPT, the magnetic coupling between W_1 and W_2 is generally weak. Hence, the self-inductance of W_1 and W_2 are approximately equal to the leakage inductance of W_1 and W_2 under a small coupling coefficient k . Therefore, the approximation, i.e., $L_{leak1} C_1 \approx L_{leak2} C_2$ is reasonable while designing a practical RIC-WPT system.

By translating (6) and (7) into a circuit model, the Lagrangian equivalent circuit of the SS topology is obtained as shown in Fig. 4. The circuit behavior for the output power and efficiency are identical as shown in Figs. 3(a) and 4 because the coordinate transformation conserves power.

C. Lagrangian Equivalent Dual Circuit of SP Topology (Steps 2 and 3)

As in the case of the SS topology, we construct the Lagrangian model of the SP topology shown in Fig. 3(b). The Lagrangian Λ_{SP} and the dissipation function D_{SP} are formulated as follows:

$$\begin{aligned} \Lambda_{SP} = & N_1 \dot{q}_1 (\phi_1 + \phi_M) + N_2 (\dot{q}_2 + \dot{q}_R) (\phi_2 - \phi_M) \\ & - \phi_1^2/2P_1 - \phi_2^2/2P_2 - \phi_M^2/2P_M - q_1^2/2C_1 \\ & - q_2^2/2C_2 + Eq_1 \end{aligned} \quad (8)$$

$$D_{SP} = R\dot{q}_R^2/2 + r_1\dot{q}_1^2/2 + r_2(\dot{q}_2 + \dot{q}_R)^2/2. \quad (9)$$

Subsequently, new variables q_a , q_b , q_c , ϕ_a , and ϕ_b are introduced as follows:

$$\begin{aligned} q_a &= \frac{N_2 C_2 q_1 + N_1 C_1 q_2}{2N_1 C_1} & q_b &= \frac{N_1 q_1 - N_2 q_2}{2N_2} \\ q_c &= \frac{q_R}{2} & \phi_a &= \frac{2P_2 (\phi_1 + \phi_2)}{P_1 + P_2} & \phi_b &= \frac{2(P_2 \phi_1 - P_1 \phi_2)}{P_1 + P_2}. \end{aligned} \quad (10)$$

We substitute (10) into (8) and (9) to obtain the following expression:

$$\begin{aligned} \Lambda_{SP} = & N_2 [(\dot{q}_a + \dot{q}_c) \phi_a + (\dot{q}_b - \dot{q}_c) \phi_b + 2(\dot{q}_b - \dot{q}_c) \phi_M] \\ & - \alpha q_a^2 / C_2 - \beta q_b^2 / C_2 - \phi_a^2 / 4\alpha P_2 - \phi_b^2 / 4\alpha P_1 \\ & - \phi_M^2 / 2P_M + \alpha N_2 E (q_a + q_b) / N_1 \end{aligned} \quad (11)$$

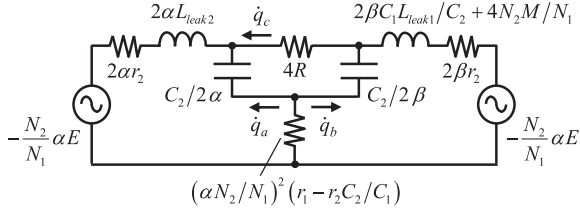


Fig. 5. Lagrangian equivalent circuit of SP topology.

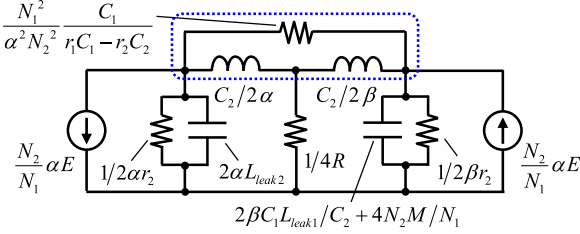


Fig. 6. Dual circuit of Fig. 5.

$$D_{SP} = 2R\dot{q}_c^2 + \alpha r_2(\dot{q}_a + \dot{q}_c)^2 + \beta r_2(\dot{q}_b - \dot{q}_c)^2 + (\alpha N_1/N_2)^2 (C_1 r_1 - C_2 r_2)(\dot{q}_a + \dot{q}_b)^2 / 2C_1. \quad (12)$$

Equations (11) and (12) are translated into Fig. 5. The output power and the efficiency of Fig. 5 are identical as shown in Fig. 3(b).

In order to discuss the quasi-duality, Fig. 5 is further transformed to obtain the equivalent dual circuit of the SP topology. Hence, the duality transformation is applied to Fig. 5 to yield Fig. 6.

D. Elucidation of Quasi-Duality (Steps 4 and 5)

As shown in Figs. 4 and 6, the circuit networks are considerably different from each other. Therefore, any duality between the SS and SP topologies is still not observed. Hence, in this subsection, we elucidate the relationship between the SS and SP topologies by further analyzing the dual circuit of the SP topology, i.e., Fig. 6.

First, we apply the Δ -Y transformation to the subcircuit denoted by the blue dashed line in Fig. 6. When the Δ -Y transformation is applied to Fig. 6, the following two approximations are introduced in addition to the already introduced approximation of $L_{leak1}C_1 \approx L_{leak2}C_2$.

- 1) The operating frequency is in the vicinity of the resonance frequency of the transmitter and the receiver. Hence, $\omega^2 \approx 1/L_1C_1 \approx 1/L_2C_2$, where ω denotes the operating angular frequency.
- 2) The Q -factor of the transmitter and the receiver, i.e., Q_1 and Q_2 , sufficiently exceeds one. Hence, $\omega L_{leak1}/r_1 \gg 1$ and $\omega L_{leak2}/r_2 \gg 1$.

Hence, we obtain Fig. 7.

Second, we further apply Thevenin's theorem to the subcircuit as denoted by the red dashed line in Fig. 7. Thus, we obtain Fig. 8. In the transformation, output power is conserved. Conversely, input power is not strictly conserved because the subcircuits

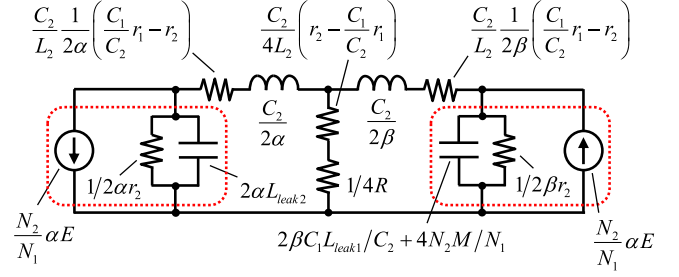
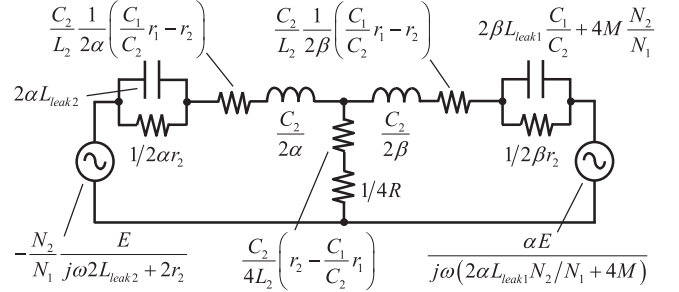

 Fig. 7. Equivalent circuit applying Δ -Y transformation to Fig. 6.


Fig. 8. Equivalent circuit applying Thevenin's theorem to Fig. 7.

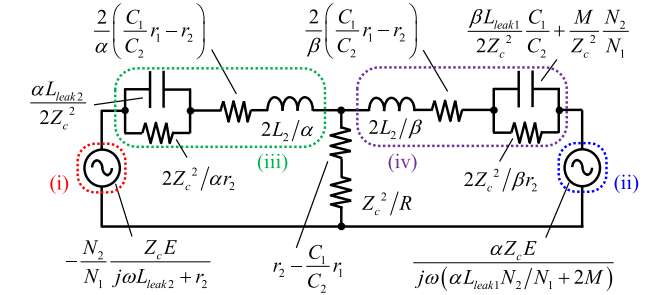


Fig. 9. Result of impedance transformation of Fig. 8.

apply Thevenin's theorem including the resistive component, i.e., $1/2\alpha r_2$ or $1/2\beta r_2$. However, based on the approximations of $Q_1 \gg 1$ and $Q_2 \gg 1$, we assume the current in $1/2\alpha r_2$ and $1/2\beta r_2$ are sufficiently lower than the current in the capacitor connected parallel to $1/2\alpha r_2$ or $1/2\beta r_2$. Therefore, the input power of Figs. 7 and 8 are approximately equal to each other. Hence, the output power and efficiency are almost identical between Figs. 7 and 8.

Subsequently, an impedance transformation is applied to Fig. 8. Specifically, the voltage and current are multiplied by $2Z_c$ and $1/2Z_c$, respectively, where Z_c is defined as $Z_c^2 \equiv L_2/C_2 \approx L_{leak2}/C_2$ and corresponds to the characteristic impedance of the receiver. Thus, we obtain Fig. 9.

Finally, we transform the subcircuits marked by the dash lines (i)–(iv) in Fig. 9 via the previously introduced approximations. The voltage sources denoted by the red (i) and blue (ii) dashed lines are correspondingly approximated as follows:

$$-\frac{N_2}{N_1} \frac{Z_c E}{j\omega L_{leak2} + r_2} = -\frac{N_2}{N_1} \sqrt{\frac{L_2}{C_2}} \frac{E}{j\omega L_{leak2} + r_2}$$

$$\begin{aligned} &\approx -\frac{N_2}{N_1} \sqrt{\frac{L_{leak2}}{C_2}} \frac{E}{j\omega L_{leak2}} \\ &\approx j \frac{N_2}{N_1} E \end{aligned} \quad (13)$$

$$\begin{aligned} \frac{\alpha Z_c E}{j\omega (\alpha L_{leak1} N_2 / N_1 + 2M)} &\approx \frac{N_1}{N_2} \sqrt{\frac{L_2}{C_2}} \frac{E}{j\omega L_{leak1}} \\ &\approx \frac{N_1}{N_2} \sqrt{\frac{L_2}{C_2}} \sqrt{\frac{C_1}{L_1}} (-jE) \\ &\approx -j \frac{N_1 C_1}{N_2 C_2} E. \end{aligned} \quad (14)$$

Subsequently, the impedance denoted by the green dash lines (iii) is defined as Z_l . The impedance Z_l is represented as follows:

$$\begin{aligned} Z_l &= 1 \left/ \left(\frac{\alpha r_2}{2Z_c^2} + j\omega \frac{\alpha L_{leak2}}{2Z_c^2} \right) \right. \\ &\quad \left. + \frac{2}{\alpha} \left(\frac{C_1}{C_2} r_1 - r_2 \right) + j\omega \frac{2L_2}{\alpha} \right. \end{aligned} \quad (15)$$

The first term in the right-hand side of (15) is approximated as follows:

$$\begin{aligned} 1 \left/ \left(\frac{\alpha r_2}{2Z_c^2} + j\omega \frac{\alpha L_{leak2}}{2Z_c^2} \right) \right. &\approx \frac{2Z_c^2}{\alpha} \frac{r_2 - j\omega L_2}{r_2^2 + \omega^2 L_2^2} \\ &\approx \frac{2Z_c^2}{\alpha} \frac{r_2}{\omega^2 L_2^2} + \frac{2Z_c^2}{\alpha} \frac{1}{j\omega L_2} \\ &\approx \frac{2}{\alpha} \left(r_2 + \frac{1}{j\omega C_2} \right). \end{aligned} \quad (16)$$

We substitute (16) into (15) to obtain the following expression:

$$Z_l \approx (2/\alpha) (r_1 C_1 / C_2 + 1/j\omega C_2 + j\omega L_{leak2}). \quad (17)$$

As in Z_l , the impedance denoted by the purple dash lines (iv) is defined as Z_r . The impedance Z_r is represented as follows:

$$\begin{aligned} Z_r &= j\omega \frac{2L_2}{\beta} + \frac{2}{\beta} \left(\frac{C_1}{C_2} r_1 - r_2 \right) \\ &\quad + 1 \left/ \left[\frac{\beta r_2}{2Z_c^2} + j\omega \left(\frac{\beta L_{leak1} C_1}{2Z_c^2 C_2} + \frac{M N_2}{Z_c^2 N_1} \right) \right] \right. \end{aligned} \quad (18)$$

The first and third terms in the right-hand side of (18) are approximated as follows:

$$\begin{aligned} j2\omega L_2 / \beta &= j2\omega L_{leak2} / \beta + j2\omega (N_2 / N_1) M / \beta \\ &\approx j2\omega L_{leak2} / \beta + j4\omega (N_2 / N_1) M / \beta^2 \end{aligned} \quad (19)$$

$$\begin{aligned} 1 \left/ \left[\frac{\beta r_2}{2Z_c^2} + j\omega \left(\frac{\beta L_{leak1} C_1}{2Z_c^2 C_2} + \frac{M N_2}{Z_c^2 N_1} \right) \right] \right. &\approx 1 \left/ \frac{\beta}{2Z_c^2} \left[r_2 + j\omega \left(L_2 + \frac{2 N_2}{\beta N_1} M \right) \right] \right. \\ &\approx \frac{2Z_c^2}{\beta} \frac{1}{r_2 + j\omega L_2} \\ &\approx (2Z_c^2 / \beta) (r_2 / \omega^2 L_2^2 - j / \omega L_2) \\ &\approx (2/\beta) (r_2 + 1/j\omega C_2). \end{aligned} \quad (20)$$

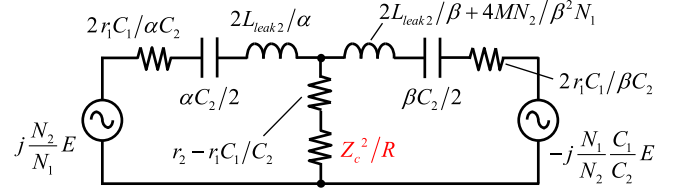


Fig. 10. Approximated equivalent dual circuit based on Fig. 9.

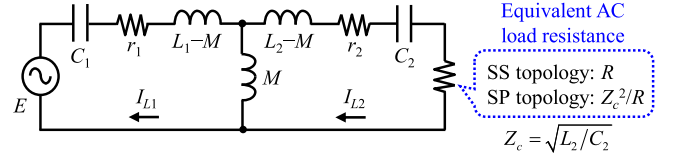


Fig. 11. Analytical model for SS and SP topologies based on quasi-duality.

We substitute (19) and (20) into (18) to obtain the following expression:

$$Z_r = j\omega \left(\frac{2L_{leak2}}{\beta} + \frac{4}{\beta^2} \frac{N_2}{N_1} M \right) + \frac{2}{\beta} \frac{C_1}{C_2} r_1 + \frac{2}{\beta} \frac{1}{j\omega C_2}. \quad (21)$$

We apply (13), (14), (17), and (21) to Fig. 9 to obtain Fig. 10. The input power and output power are almost conserved via the process of deriving Fig. 10. Therefore, Fig. 10 approximately works as the dual circuit of the SP topology.

Figs. 4 and 10 show the same topology and the same parameters with the exception of the equivalent ac load resistance. Strictly speaking, the parameter of the voltage sources of Fig. 10 includes the imaginary unit j . However, the phase relation between the two voltage sources in the equivalent circuit is identical in Figs. 4 and 10. Therefore, with respect to the case of analyzing the input power and output power per unit time, the difference due to the presence or absence of the imaginary unit is ignored.

Based on Figs. 4 and 10, the SP topology of the RIC-WPT system approximately behaves as the dual of the SS topology in which the equivalent ac load resistance R is replaced by Z_c^2/R . The relation is termed as the quasi-duality. Based on the quasi-duality, the output power and efficiency of the SP topology [see Fig. 3(b)] are calculated via the original equivalent circuit of the SS topology [see Fig. 3(a)]. The insight offers a straightforward comparison between the SS and SP topologies.

III. PROPOSED STRATEGY OF TOPOLOGY SELECTION BASED ON QUASI-DUALITY

Fig. 11 shows the unified analysis model for the SS and SP topologies based on quasi-duality. For the calculation of the output power and efficiency of the SS topology, the equivalent ac load resistance should be set at R . On the other hand, for the calculation of the SP topology, the equivalent ac load resistance should be set at Z_c^2/R . In this section, we propose a strategy of the topology selection between the SS and SP topologies based on the following three steps.

- 1) Based on Fig. 11, we derive the output power P_o and efficiency η of the SS and SP topologies by referring to [31].
- 2) We derive the boundary resistance of P_o , i.e., the equivalent ac load resistance wherein the superiority in terms of P_o of the SS and SP topologies are exchanged. Subsequently, based on the boundary resistance of P_o , we propose the strategy of the topology selection in terms of P_o .
- 3) As in step 2, we derive the boundary resistance of η , i.e., the equivalent ac load resistance by which the superiority in terms of η of the SS and SP topologies are exchanged. Subsequently, based on the boundary resistance of η , we propose the strategy of the topology selection in terms of η .

A. Derivation of Output Power and Efficiency of SS and SP Topologies (Step 1)

First, we set the equivalent ac load resistance to R . Based on Kirchhoff's voltage law, Fig. 11 is described as follows:

$$\begin{aligned} E &= (r_1 + jX_1) I_{L1} + j\omega M (I_{L1} - I_{L2}) \\ j\omega M (I_{L1} - I_{L2}) &= [(r_2 + R) + jX_2] I_{L2} \end{aligned} \quad (22)$$

where jX_1 and jX_2 are defined as follows:

$$\begin{aligned} jX_1 &= j(\omega L_1 - 1/\omega C_1) \\ jX_2 &= j(\omega L_2 - 1/\omega C_2). \end{aligned} \quad (23)$$

Subsequently, from (22) and (23), the transmitter current I_{L1} and the receiver current I_{L2} are correspondingly derived as follows:

$$\begin{aligned} I_{L1} &= E (N_{1R} + jN_{1I}) / D_p \\ I_{L2} &= E (N_{2R} + jN_{2I}) / D_p \end{aligned} \quad (24)$$

where N_{1R} , N_{1I} , N_{2R} , N_{2I} , and D_p are defined as follows:

$$\begin{aligned} N_{1R} &= \omega^2 M^2 (r_2 + R) + r_1 [(r_2 + R)^2 + X_2^2] \\ N_{1I} &= \omega^2 M^2 X_2 - X_1 [(r_2 + R)^2 + X_2^2] \\ N_{2R} &= \omega M [X_1 (r_2 + R) + X_2 r_1] \\ N_{2I} &= \omega M [\omega^2 M^2 + r_1 (r_2 + R) - X_1 X_2] \\ D_p &= 2\omega^2 M^2 [r_1 (r_2 + R) - X_1 X_2 + \omega^2 M^2 / 2] \\ &\quad + (r_1^2 + X_1^2) [(r_2 + R)^2 + X_2^2]. \end{aligned} \quad (25)$$

From (24) and (25), the input power P_i and output power P_o are correspondingly derived as follows:

$$P_i = \text{Re}(E \cdot \bar{I}_{L1}) = E^2 N_{1R} / D_p \quad (26)$$

$$\begin{aligned} P_o &= R \cdot I_{L2} \cdot \bar{I}_{L2} = RE^2 \omega^2 M^2 / D_p \\ &= RE^2 \omega^2 M^2 \frac{2\omega^2 M^2 [r_1 (r_2 + R) - X_1 X_2 + \omega^2 M^2 / 2]}{(r_1^2 + X_1^2) [(r_2 + R)^2 + X_2^2]}. \end{aligned} \quad (27)$$

By dividing the output power by the input power, η is derived as follows:

$$\begin{aligned} \eta &= P_o / P_i = R\omega^2 M^2 / N_{1R} \\ &= \frac{R\omega^2 M^2}{\omega^2 M^2 (r_2 + R) + r_1 [(r_2 + R)^2 + X_2^2]}. \end{aligned} \quad (28)$$

Subsequently, we define the equivalent ac load resistance values to achieve the maximum P_o and maximum η as $R_{SS_p\max}$ and $R_{SS_η\max}$. From (27) and (28), $R_{SS_p\max}$ and $R_{SS_η\max}$ are derived as resistance values that satisfy $\partial P_o / \partial R = 0$ and $\partial \eta / \partial R = 0$, respectively. Therefore, $R_{SS_p\max}$ and $R_{SS_η\max}$ are derived as follows:

$$R_{SS_p\max} = \sqrt{\frac{2\omega^2 M^2 (r_1 r_2 - X_1 X_2) + \omega^4 M^4}{r_1^2 + X_1^2} + r_2^2 + X_2^2} \quad (29)$$

$$R_{SS_η\max} = \sqrt{\omega^2 M^2 r_2 / r_1 + r_2^2 + X_2^2}. \quad (30)$$

Equations (22)–(30) correspond to the common analysis results of the SS topology. The analysis results are well known [31], [32].

However, based on the quasi-duality, the input power, output power, and efficiency of the SP topology are easily calculated by replacing only the equivalent ac load resistance R of (26)–(28) with Z_c^2 / R . Additionally, based on the quasi-duality, the resistance $R_{SP_p\max}$ to achieve the maximum power of the SP topology and resistance $R_{SP_η\max}$ to achieve the maximum efficiency of the SP topology are easily derived as follows:

$$R_{SP_p\max} = Z_c^2 / R_{SS_p\max} \quad R_{SP_η\max} = Z_c^2 / R_{SS_η\max}. \quad (31)$$

The maximum output power of the SS and SP topologies are identical due to the maximum power of Fig. 11 corresponding to the maximum power of both the topologies. Similarly, the maximum efficiency of the SS and SP topologies are identical. The insights follow those derived in extant studies [13].

B. Proposed Strategy of Topology Selection in Terms of Output Power (Step 2)

Subsequently, we derive the boundary resistance for the output power. In order to ensure the simplicity of the calculation, we divide the denominator and numerator of (27) by R . Thus, the terms for R appear only in the denominator. Subsequently, we extract only the terms for R in the denominator and define the sum of the terms as x . Furthermore, we denote x as x_{SS} when the equivalent ac load resistance is set at R , whereas we denote x as x_{SP} when the equivalent ac load resistance is set at Z_c^2 / R . Thus, x_{SS} and x_{SP} are derived as follows:

$$\begin{aligned} x_{SS} &= \omega^2 M^2 [2(r_1 r_2 - X_1 X_2) + \omega^2 M^2] / R \\ &\quad + (r_1^2 + X_1^2) [(r_2^2 + X_2^2) / R + R] \end{aligned} \quad (32)$$

$$\begin{aligned} x_{SP} &= \omega^2 M^2 [2(r_1 r_2 - X_1 X_2) + \omega^2 M^2] R / Z_c^2 \\ &\quad + (r_1^2 + X_1^2) [(r_2^2 + X_2^2) R / Z_c^2 + Z_c^2 / R]. \end{aligned} \quad (33)$$

TABLE I
APPROPRIATE TOPOLOGY TO ACHIEVE HIGHER OUTPUT POWER

	Equivalent AC load resistance R	Output Power P_o
$R_{SS_pmax} < Z_c$	$R < Z_c$	SS topology > SP topology
	$R = Z_c$	SS topology = SP topology
	$R > Z_c$	SS topology < SP topology
$R_{SS_pmax} = Z_c$	Load Independent	SS topology = SP topology
$R_{SS_pmax} > Z_c$	$R < Z_c$	SS topology < SP topology
	$R = Z_c$	SS topology = SP topology
	$R > Z_c$	SS topology > SP topology

The magnitude relation of the output power between SS and SP topologies is calculated via analyzing the magnitude relation between x_{SS} and x_{SP} .

In order to discuss the magnitude relation between x_{SS} and x_{SP} , we calculate $x_{SS} - x_{SP}$. If $x_{SS} - x_{SP} < 0$, the SS topology achieves higher output power than the SP topology. Conversely, if $x_{SS} - x_{SP} > 0$, the SP topology achieves higher output power than the SS topology. Furthermore, if $x_{SS} - x_{SP} = 0$, the output powers of the SS and SP topologies are identical. Subsequently, $x_{SS} - x_{SP}$ is calculated as follows:

$$x_{SS} - x_{SP} = (r_1^2 + X_1^2) (Z_c^2 - R_{SS_pmax}^2) \times (R/Z_c^2 - 1/R). \quad (34)$$

The factor of $(r_1^2 + X_1^2)$ in the right-hand side of (34) is always positive. Therefore, the sign of $x_{SS} - x_{SP}$ is determined by the signs of $(Z_c^2 - R_{SS_pmax}^2)$ and $(R/Z_c^2 - 1/R)$. Thus, an appropriate topology to achieve higher output power is only determined via the magnitude relationship between Z_c and R_{SS_pmax} and the magnitude relationship between Z_c and R . Therefore, the boundary resistance for the output power corresponds to Z_c . Finally, an appropriate topology to achieve higher output power is summarized as shown in Table I.

From Table I, Z_c denotes the critical factor to select an appropriate topology in terms of the output power. Generally, the SS topology is appropriate when the equivalent ac load resistance is low, and the SP topology is appropriate when the equivalent ac load resistance is high [6]. However, Table I indicates that this common knowledge is not always the case.

C. Proposed Strategy of Topology Selection in Terms of Efficiency (Step 3)

As in the case of the output power, we derive the boundary resistance for efficiency. First, we divide the denominator and numerator of (28) by R . Thus, the terms for R appear only in the denominator. Subsequently, we extract only the terms for R in the denominator and we define the sum of the terms as y . Furthermore, we denote y as y_{SS} when the equivalent ac load

TABLE II
APPROPRIATE TOPOLOGY TO ACHIEVE HIGHER EFFICIENCY

	Equivalent AC load resistance R	Efficiency η
$R_{SS_ηmax} < Z_c$	$R < Z_c$	SS topology > SP topology
	$R = Z_c$	SS topology = SP topology
	$R > Z_c$	SS topology < SP topology
$R_{SS_ηmax} = Z_c$	Load Independent	SS topology = SP topology
$R_{SS_ηmax} > Z_c$	$R < Z_c$	SS topology < SP topology
	$R = Z_c$	SS topology = SP topology
	$R > Z_c$	SS topology > SP topology

resistance is set at R , whereas we define y as y_{SP} when the equivalent ac load resistance is set at Z_c^2/R . Thus, y_{SS} and y_{SP} are derived as follows:

$$y_{SS} = [\omega^2 M^2 r_2 + r_1 (r_2^2 + X_2^2)] / R + r_1 R \quad (35)$$

$$y_{SP} = [\omega^2 M^2 r_2 + r_1 (r_2^2 + X_2^2)] R / Z_c^2 + r_1 Z_c^2 / R. \quad (36)$$

The magnitude relation of the efficiency between the SS and SP topologies is calculated via analyzing the magnitude relation between y_{SS} and y_{SP} .

In order to discuss the magnitude relation between y_{SS} and y_{SP} , we calculate $y_{SS} - y_{SP}$. If $y_{SS} - y_{SP} < 0$, the SS topology achieves higher efficiency than the SP topology. Conversely, if $y_{SS} - y_{SP} > 0$, the SP topology achieves higher efficiency than the SS topology. Furthermore, if $y_{SS} - y_{SP} = 0$, the efficiencies of the SS and SP topologies are identical. Subsequently, $y_{SS} - y_{SP}$ is calculated as follows:

$$y_{SS} - y_{SP} = r_1 (Z_c^2 - R_{SS_ηmax}^2) (R/Z_c^2 - 1/R). \quad (37)$$

As in (34), the sign of $y_{SS} - y_{SP}$ is only determined by the magnitude relationship between Z_c and $R_{SS_ηmax}$ and the magnitude relationship between Z_c and R . Therefore, the boundary resistance for the efficiency corresponds to Z_c . The boundary resistances for the output power and efficiency are identical to each other. Finally, an appropriate topology to achieve higher efficiency is summarized as shown in Table II.

However, when we compare the efficiency between the SS and SP topologies, we should consider only the condition of $R_{SS_ηmax} < Z_c$. In several practical RIC-WPT systems, $R_{SS_ηmax}$ is typically lower than Z_c . Subsequently, we calculate $R_{SS_ηmax}^2 - Z_c^2$ to show that the magnitude relationship of $R_{SS_ηmax} < Z_c$ is satisfied in several practical RIC-WPT systems. Based on the already introduced approximations, $R_{SS_ηmax}^2 - Z_c^2$ is expressed as follows:

$$\begin{aligned} R_{SS_ηmax}^2 - Z_c^2 &= (\omega^2 M^2 r_2 / r_1 + r_2^2 + X_2^2) - L_2 / C_2 \\ &\approx (\omega^2 k^2 L_1 L_2 r_2 / r_1 + r_2^2) - \omega^2 L_2^2 \\ &= r_2^2 (k^2 Q_1 Q_2 + 1 - Q_2^2) \end{aligned}$$

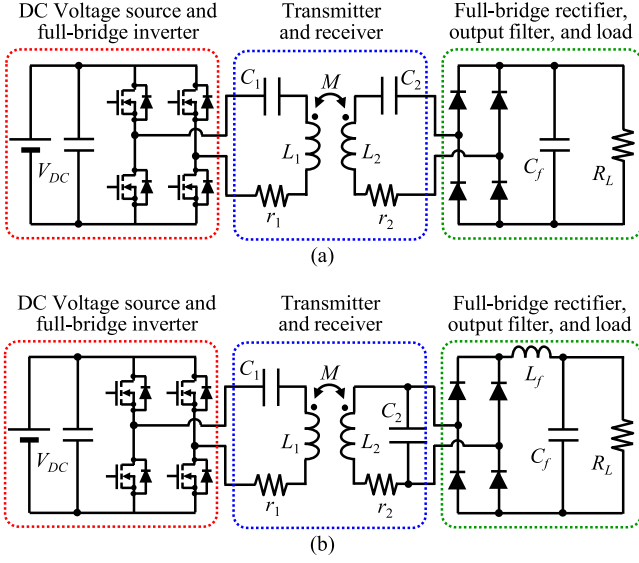


Fig. 12. Circuit configurations for experiments. (a) SS topology. (b) SP topology.

$$\approx r_2^2 Q_1 Q_2 (k^2 - Q_2/Q_1). \quad (38)$$

In order to satisfy $R_{SS_p\max}^2 - Z_c^2 < 0$ (i.e., $R_{SS_p\max} < Z_c$), the factor of $k^2 - Q_2/Q_1$ must be negative. In several practical RIC-WPT systems, the coupling coefficient k is typically less than 0.3. Therefore, k^2 tends to be 0.1 or less. Conversely, Q_2/Q_1 typically exceeds 0.1. Generally, it is a rare case that Q_1 is ten or more times than Q_2 . It should be noted that Q_2 was defined as nonload Q -factor in Section II. Hence, the condition of $R_{SS_p\max} \geq Z_c$ is typically ignored.

Tables I and II denote the proposed strategy of the topology selection based on quasi-duality. The resistances of $R_{SS_p\max}$ and $R_{SS_q\max}$ are well known in RIC-WPT studies. Therefore, based on the proposed strategy, we easily understand which topology achieves higher performance by only comparing the simple resistances after designing the transmitting and receiving coils.

IV. VERIFICATION

In this section, we perform experiments to achieve the following two purposes.

- 1) We verify the appropriateness of the unified analysis model shown in Fig. 11.
- 2) We verify the appropriateness and the effectiveness of the proposed strategy of the topology selection shown in Tables I and II.

Fig. 12 shows the circuit configurations for the experiment related to SS and SP topologies. Furthermore, Fig. 13 shows the photograph of the experimental setup of the SS topology. In the experiment, the ac sinusoidal voltage source in the equivalent circuit is generated by the dc voltage source and the full-bridge inverter. The voltage generated by the full-bridge inverter corresponds to a rectangular waveform. However, when

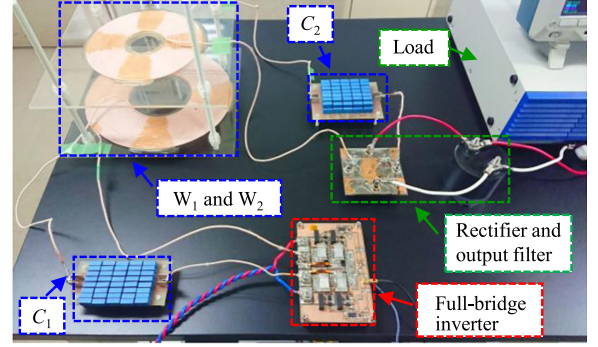


Fig. 13. Photograph of experimental setup for SS topology.

the quality factor of the transmitter sufficiently exceeds one, the rectangular waveform is assumed as a sinusoidal wave wherein the amplitude corresponds to a fundamental wave [4], [15].

In this experiment, the load is configured as the rectifying circuit with the load resistance R_L . Therefore, the equivalent ac load resistance R is not identical to R_L . In general, R is affected not only by R_L but also by the output filter C_f and L_f [19]. However, in order to simplify the relation between R and R_L , we designed C_f and L_f to be sufficiently large so that the voltage of C_f and the current through L_f are almost constant. In this case, R is simply dependent only on R_L . According to [33], the relation between R and R_L can be expressed by (39) in the case of the SS topology and by (40) in the case of the SP topology as follows:

$$R = \frac{8}{\pi^2} R_L \quad (39)$$

$$R = \frac{\pi^2}{8} R_L. \quad (40)$$

Subsequently, in the experiment and the theoretical analysis, C_2 of the SS and SP topologies are selected to resonate with L_2 at a designed resonance frequency f_0 . Therefore, C_2 uses the same value for the SS and SP topologies. Conversely, C_1 of the SS and SP topologies are selected to achieve a unity power factor at f_0 after determining C_2 [2], [3], [5], [12]. Thus, C_1 of the SS and SP topologies are determined as follows:

$$C_{1_SS} = L_2 C_2 / L_1, \quad C_{1_SP} = L_2 C_2 / L_1 (1 - k^2) \quad (41)$$

where C_{1_SS} corresponds to C_1 for the SS topology and C_{1_SP} corresponds to C_1 for the SP topology. Therefore, C_{1_SS} and C_{1_SP} are different from each other. It should be noted that (41) satisfies the approximations of $L_{leak1} C_1 \approx L_{leak2} C_2$ and $1/L_1 C_1 \approx 1/L_2 C_2$ introduced in Section II when k is sufficiently smaller than one.

Table III shows the circuit parameters of the transmitter and receiver used in this section. As shown in Table III, r_2 only includes the parasitic resistance of W_2 . Conversely, r_1 includes the output resistance of the full-bridge inverter ($=0.022 \Omega$), parasitic resistance of the resonance capacitor ($=0.018 \Omega$), and parasitic resistance of W_1 ($=0.160 \Omega$). When the efficiency is

TABLE III
CIRCUIT PARAMETERS FOR RESONATORS

Symbols / Parameters		Values
L_1	Self-inductance of W_1	140.90 μH
L_2	Self-inductance of W_2	55.20 μH
M	Mutual inductance between W_1 and W_2	8.73 μH
k	Coupling coefficient between W_1 and W_2	0.099
r_1	Whole parasitic resistance of transmitter	0.200 Ω
r_2	Parasitic resistance of W_2 only	0.084 Ω
f_0	Designed resonance frequency	105.0 kHz
Q_1	Q -factor of transmitter	464.8
Q_2	Non-load Q -factor of receiver	433.5
C_f	Capacitance of output filter	100 μF
L_f	Inductance of output filter	1.1 mH
C_{1_SS}	Capacitance of transmitter (Theory)	16.31 nF
	(Experiment)	16.23 nF
C_{1_SP}	Capacitance of transmitter (Theory)	16.47 nF
	(Experiment)	16.45 nF
C_2	Capacitance of receiver (Theory)	41.62 nF
	(Experiment)	41.47 nF

TABLE IV
CIRCUIT PARAMETERS FOR VERIFICATION OF APPROPRIATENESS OF UNIFIED ANALYSIS MODEL

Symbols / Parameters		Values
V_{DC}	Input DC voltage	20 V
R	Load resistance	100.0 Ω , 249.7 Ω , 1011.2 Ω

low, the transmitter current is typically high. Thus, the output power is especially affected by r_1 . Therefore, we accurately model r_1 to calculate the accurate output power in low-efficiency conditions.

A. Appropriateness of Unified Analysis Model (Fig. 11)

In this subsection, we demonstrate that the output power and the efficiency of the SP topology are calculated using the unified analysis model of Fig. 11 according to quasi-duality. As discussed in Section II, Fig. 11 is derived using the coordinate transformation of the Lagrangian model and a few practically acceptable approximations. Therefore, the appropriateness of Fig. 11 should be validated not only in comparison with the theoretically calculated performance of the original equivalent circuit, i.e., Fig. 3(b) but also in comparison with the experimentally evaluated performance of the prototype circuit, i.e., Fig. 12(b). Consequently, the output power and the efficiency are compared among the following three circuits: Fig. 11 with the equivalent ac load resistance set as Z_c^2/R , Fig. 3(b), and Fig. 12(b).

Tables III and IV show the circuit parameters in the evaluation in this subsection. We adopt three types of R to show that the unified analysis model of Fig. 11 is valid irrespective of the frequency splitting phenomenon. When R is set as 100 Ω , the

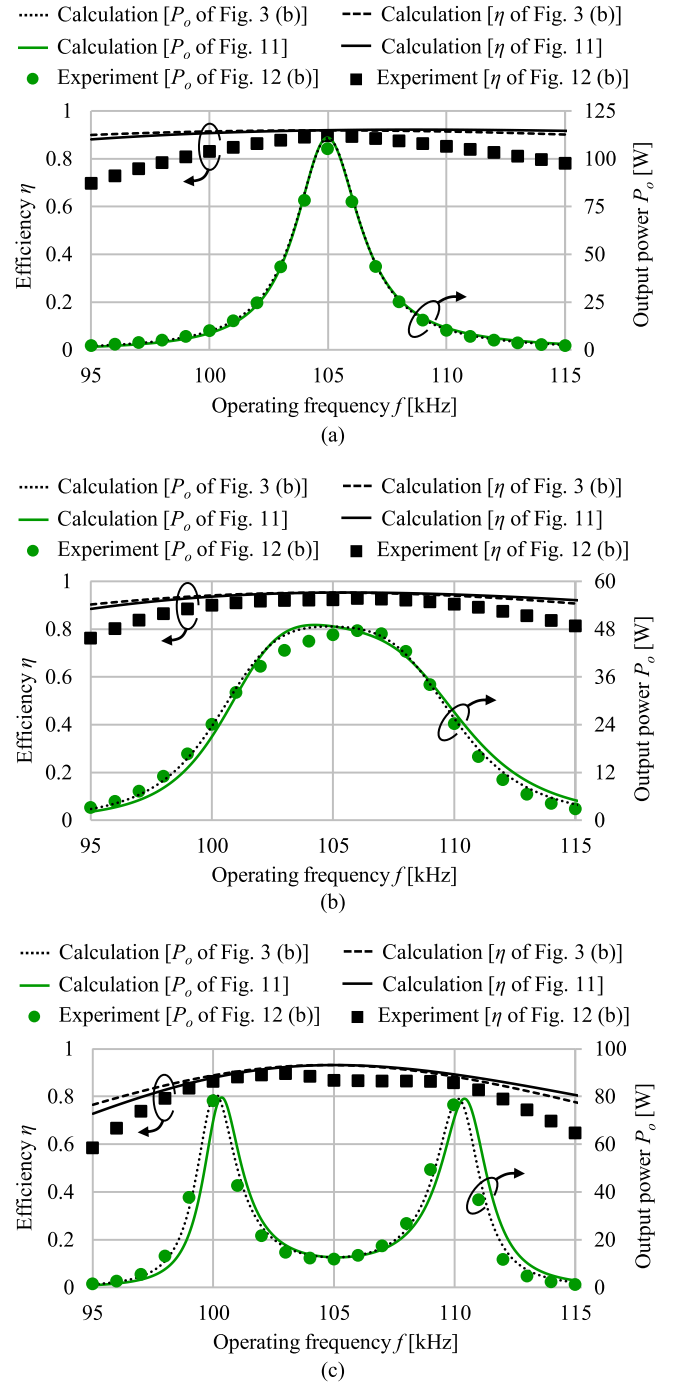


Fig. 14. Verification of appropriateness of unified analysis model. (a) $R = 100.0 \Omega$. (b) $R = 249.7 \Omega$. (c) $R = 1011.2 \Omega$.

frequency splitting phenomenon does not occur. Conversely, when R is set as 249.7 or 1011.2 Ω , the frequency splitting phenomenon occurs. Specifically, the frequency splitting phenomenon significantly occurs when R is set as 1011.2 Ω .

Subsequently, Fig. 14 shows the output power and the efficiency of the SP topology based on the operating frequency f . In Fig. 14, the dashed lines denote the theoretical analysis

TABLE V
CIRCUIT PARAMETERS FOR VERIFICATION OF APPROPRIATENESS OF PROPOSED
STRATEGY OF TOPOLOGY SELECTION

	Symbols / Parameters		Values
Condition 1	V_{DC}	Input DC voltage	6 V
	f	(Theory)	105.00 kHz
		Operating frequency (Experiment of SS topology) (Experiment of SP topology)	105.09 kHz 104.95 kHz
Condition 2	V_{DC}	Input DC voltage	18 V
	f	(Theory)	107.00 kHz
		Operating frequency (Experiment of SS topology) (Experiment of SP topology)	107.00 kHz 107.00 kHz

results derived from the original equivalent circuit of the SP topology shown in Fig. 3(b); solid lines denote the theoretical analysis results derived from the equivalent circuit of Fig. 11, in which, the equivalent ac load resistance is set as Z_c^2/R ; and markers denote the experimental results in Fig. 12(b). In this study, detailed derivation processes of the theoretical analysis of Fig. 3(b) are excluded because the processes are based on general circuit theory.

As shown in the theoretical analysis results of Fig. 14, Figs. 3(b) and 11 almost exhibit the same frequency dependence between the output power and efficiency. Strictly speaking, the calculated results of Fig. 11 slightly deviate from the calculated results of Fig. 3(b) when the frequency splitting phenomenon significantly occurs. However, Fig. 11 comparatively accurately estimates the output power and efficiency in the SP topology at frequencies corresponding to the multiple resonance modes.

Additionally, the experimental results match well with the theoretical analysis results in the vicinity of the frequencies corresponding to f_0 and multiple resonance modes. Practical RIC-WPT systems are typically operated in the vicinity of the frequencies corresponding to f_0 and multiple resonance modes. Therefore, the results support the appropriateness and practical use of the unified analysis model.

Furthermore, the unified analysis model does not exhibit a limit on the output power because any approximation for the output power was not introduced when the unified analysis model was derived. Hence, the unified analysis model is applied to various applications irrespective of the output power.

B. Appropriateness and Effectiveness of the Proposed Strategy of Topology Selection (Tables I and II)

Subsequently, we demonstrate that an appropriate topology between the SS and SP topologies is selected by only comparing simple resistance values. Tables III and V show the circuit parameters used in the evaluation of this subsection. As shown in Table V, we perform the evaluations under two conditions. The first condition satisfies $Z_c < R_{SS_pmax}$ and $R_{SS_ηmax} < Z_c$. The second condition satisfies

$R_{SS_pmax} < Z_c$ and $R_{SS_ηmax} < Z_c$. In condition 1, f is set as the frequency in which the inverter achieves the unity power factor. Therefore, in the case of the theoretical analysis, f_0 is 105.00 kHz. Additionally, f for the experiment of the SS topology corresponds to 105.09 kHz, and f for the experiment of the SP topology corresponds to 104.95 kHz. The characteristic of the RIC-WPT system is sensitive relative to the slight variation in the resonant frequencies when f is set as the frequency in which the inverter achieves the unity power factor. Therefore, f is accurately adjusted by considering the error of the parameters of the resonators. Conversely, in condition 2, f is set as 107.00 kHz. In this case, f for the theoretical analysis and experiment are identical because f is relatively far from the frequency at which the inverter achieves the unity power factor.

Subsequently, Fig. 15 shows the output power and efficiency of the SS and SP topologies based on the equivalent ac load resistance under the two conditions. In Fig. 15, the solid and dashed lines denote the theoretical analysis results and markers denote the experimental results. As shown in Fig. 15, an appropriate topology between SS and SP topologies is interchanged with Z_c as the boundary. Furthermore, Fig. 15 shows that an appropriate topology to achieve higher output power also depends on the magnitude relation between Z_c and R_{SS_pmax} . The results are consistent with those in Tables I and II. Therefore, it is confirmed that an appropriate topology is selected by comparing only simple resistances.

Finally, we discuss applicable ranges of the proposed strategy for the topology selection. In Section II, we introduced three approximations for the coupling coefficient, operating frequency, and Q -factor to elucidate the quasi-duality. Therefore, there are applicable ranges in the proposed strategy. Among the approximations, the approximation for the Q -factor is usually satisfied. The output power and efficiency of the RIC-WPT are well known to be higher as the Q -factor is higher [3], [6]. Therefore, the Q -factor is typically designed as higher, and thus, Q_1 and Q_2 sufficiently exceed one in practical RIC-WPT systems [2]. Therefore, when we use the proposed strategy of topology selection, it is typically necessary to consider only the approximations for the coupling coefficient and operating frequency.

Fig. 16 shows the theoretical calculation results of the output power and the efficiency of the SS and SP topologies under various practically achievable coupling coefficients. Fig. 16(a) shows the results at $ff_0 = 1.00$ at $V_{DC} = 5$ V; and Fig. 16(b) shows the results at $ff_0 = 1.14$ at $V_{DC} = 20$ V. In each of these operating conditions, the SS and SP topologies were calculated and compared under the same V_{DC} , although V_{DC} was set at different values between these two operating conditions so that the calculated output power at Z_c becomes within the range of 0.1–100 W.

As shown in Fig. 16, the proposed strategy of topology selection in Tables I and II is approximately effective even if the operating frequency slightly deviates from the resonant frequency. Furthermore, the proposed strategy is also approximately effective under a wide range of coupling coefficients.

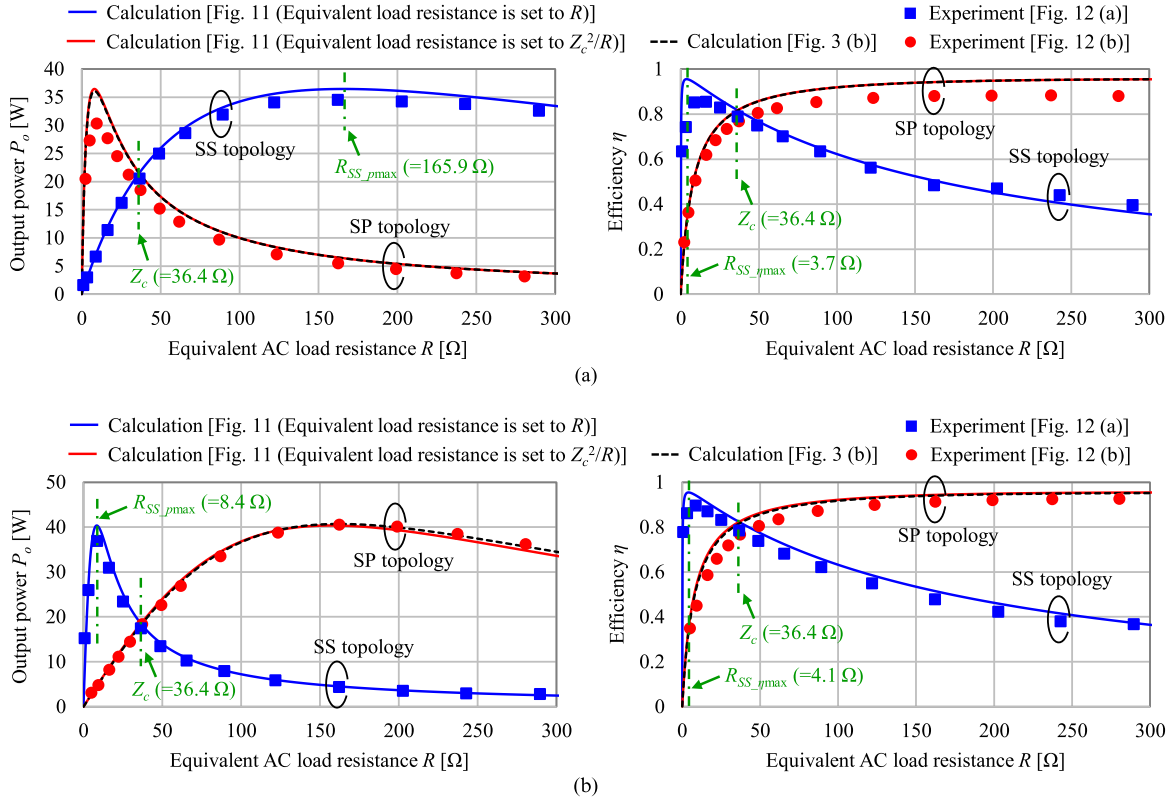


Fig. 15. Comparison of P_o and η between SS and SP topology. (a) Condition 1 ($Z_c < R_{SS_pmax}$ and $R_{SS_ηmax} < Z_c$). (b) Condition 2 ($R_{SS_pmax} < Z_c$ and $R_{SS_ηmax} < Z_c$).

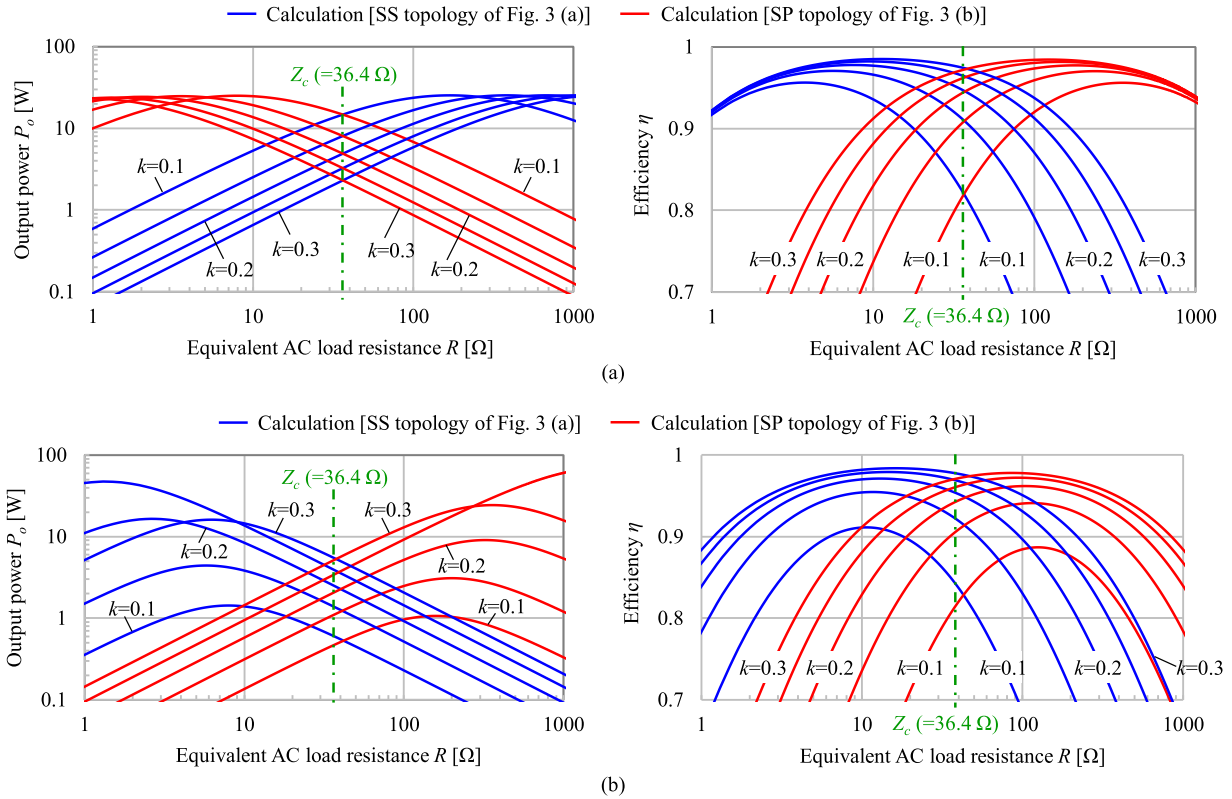


Fig. 16. Comparison of P_o and η between SS and SP topology under various k ($k = 0.1, \dots, 0.3$, steps of 0.05). (a) $f/f_0 = 1.00$ and $V_{DC} = 5$ V. (b) $f/f_0 = 1.14$ and $V_{DC} = 20$ V.

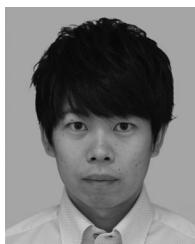
V. CONCLUSION

It is typically difficult to select an appropriate topology between SS and SP topologies because the topologies are usually analyzed and designed based on a different equivalent circuit. In order to address this issue, in this study, we first elucidated the quasi-duality between the SS and SP topologies, which indicates that the output power and efficiency of the SP topology were analyzed via the equivalent circuit of the SS topology. Subsequently, based on this knowledge, we proposed a straightforward strategy of topology selection. Based on the proposed strategy, an appropriate topology can be selected by comparing only the equivalent ac load resistance, characteristic impedance, and ac load resistance that can achieve the maximum efficiency or maximum output power of the SS topology. Furthermore, the appropriateness and effectiveness of the proposed strategy were successfully confirmed via experiments. Finally, we concluded that the proposed strategy is promising in terms of selecting an appropriate topology to achieve higher output power or efficiency at the beginning of the RIC-WPT design.

The proposed strategy is limited to the topology selection between the SS and SP topologies because only the quasi-duality between the SS and SP topologies have been elucidated using the Lagrangian dynamics. However, similar strategies may be derived for other topologies, if the Lagrangian dynamics are applied to elucidate the quasi-duality or similar relations for these other topologies.

REFERENCES

- [1] N. Liu and T. G. Habetler, "Design of a universal inductive charger for multiple electric vehicle models," *IEEE Trans. Power Electron.*, vol. 30, no. 11, pp. 6378–6390, Nov. 2015.
- [2] C.-S. Wang, G. A. Covic, and O. H. Stielau, "Power transfer capability and bifurcation phenomena of loosely coupled inductive power transfer systems," *IEEE Trans. Ind. Electron.*, vol. 51, no. 1, pp. 148–157, Feb. 2004.
- [3] S. Li and C. C. Mi, "Wireless power transfer for electric vehicle applications," *IEEE Trans. Emerg. Sel. Topics Power Electron.*, vol. 3, no. 1, pp. 4–17, Mar. 2015.
- [4] M. Fu, Z. Tang, and C. Ma, "Analysis and optimized design of compensation capacitors for a megahertz WPT system using full-bridge rectifier," *IEEE Trans. Ind. Inform.*, vol. 15, no. 1, pp. 95–104, Jan. 2019.
- [5] I. Ortega-Isasa, K. P. Benli, F. Casado, J. I. Sancho, and D. Valderas, "Topology analysis of wireless power transfer systems manufactured via inkjet printing technology," *IEEE Trans. Ind. Electron.*, vol. 64, no. 10, pp. 7749–7757, Oct. 2017.
- [6] M. Schormans, V. Valente, and A. Demosthenous, "Practical inductive link design for biomedical wireless power transfer: A tutorial," *IEEE Trans. Biomed. Circuits Syst.*, vol. 12, no. 5, pp. 1112–1130, Jul. 2018.
- [7] M. E. Halpern and D. C. Ng, "Optimal tuning of inductive wireless power links: Limits of performance," *IEEE Trans. Circuits Syst. I, Reg. Papers*, vol. 62, no. 3, pp. 725–732, Mar. 2015.
- [8] A. J. Moradewicz and M. P. Kazmierkowski, "Contactless energy transfer system with FPGA-controlled resonant converter," *IEEE Trans. Ind. Electron.*, vol. 57, no. 9, pp. 3181–3190, Sep. 2010.
- [9] M. Ishihara, K. Umetani, and E. Hiraki, "Elucidation of quasi-duality between series-series and series-parallel topologies of resonant inductive coupling wireless power transfer systems," in *Proc. IEEE Power Electron. Drive Syst. Conf.*, Honolulu, HI, USA, 2017, pp. 674–679.
- [10] K. Aditya and S. S. Williamson, "Design guidelines to avoid bifurcation in a series-series compensated inductive power transfer system," *IEEE Trans. Ind. Electron.*, vol. 66, no. 5, pp. 3973–3982, May 2019.
- [11] Y. H. Sohn, B. H. Choi, G.-H. Cho, and C. T. Rim, "Gyrator-based analysis of resonant circuits in inductive power transfer systems," *IEEE Trans. Power Electron.*, vol. 31, no. 10, pp. 6824–6843, Oct. 2016.
- [12] M. Kim, J.-W. Lee, and B. K. Lee, "Practical bifurcation criteria considering inductive power pad losses in wireless power transfer systems," *J. Elect. Eng. Technol.*, vol. 12, no. 1, pp. 173–181, Jan. 2017.
- [13] R. Jegadeesan and Y.-X. Guo, "Topology selection and efficiency improvement of inductive power links," *IEEE Trans. Antennas Propag.*, vol. 60, no. 10, pp. 4846–4854, Oct. 2012.
- [14] H. Matsumoto, Y. Neba, and H. Asahara, "Switched compensator for contactless power transfer systems," *IEEE Trans. Power Electron.*, vol. 30, no. 11, pp. 6120–6129, Nov. 2015.
- [15] W. Zhang, S.-C. Wong, C. K. Tse, and Q. Chen, "Analysis and comparison of secondary series- and parallel-compensated inductive power transfer systems operating for optimal efficiency and load-independent voltage-transfer ratio," *IEEE Trans. Power Electron.*, vol. 29, no. 6, pp. 2979–2990, Jun. 2014.
- [16] W. Zhang, S.-C. Wong, C. K. Tse, and Q. Chen, "Load-independent duality of current and voltage outputs of a series- or parallel-compensated inductive power transfer converter with optimized efficiency," *IEEE Trans. Emerg. Sel. Topics Power Electron.*, vol. 3, no. 1, pp. 137–146, Mar. 2015.
- [17] W.-Q. Niu, J.-X. Chu, W. Gu, and A.-D. Shen, "Exact analysis of frequency splitting phenomena of contactless power transfer systems," *IEEE Trans. Circuits Syst. I, Reg. Papers*, vol. 60, no. 6, pp. 1670–1677, Jun. 2013.
- [18] R. Huang, B. Zhang, D. Qiu, and Y. Zhang, "Frequency splitting phenomena of magnetic resonant coupling wireless power transfer," *IEEE Trans. Magn.*, vol. 50, no. 11, Nov. 2014, Art. no. 8600204.
- [19] O. Knecht and J. W. Kolar, "Comparative evaluation of IPT resonant circuit topologies for wireless power supplies of implantable mechanical circulatory support systems," in *Proc. Appl. Power Electron. Conf. Expo.*, Tampa, FL, USA, 2017, pp. 3271–3278.
- [20] S. D. Freeland, "Techniques for the practical application of duality to power circuits," *IEEE Trans. Power Electron.*, vol. 7, no. 2, pp. 374–384, Apr. 1992.
- [21] K. Umetani, "Lagrangian method for deriving electrically dual power converters applicable to nonplanar circuit topologies," *IEEE Trans. Elect. Electron. Eng.*, vol. 11, no. 4, pp. 521–530, May 2016.
- [22] Z. H. Bai and Z. C. Zhang, "Conformation of multilevel current source converter topologies using the duality principle," *IEEE Trans. Power Electron.*, vol. 23, no. 5, pp. 2260–2267, Sep. 2008.
- [23] J. W. Kolar, H. Ertl, and F. Zach, "Quasi-dual modulation of three-phase PWM converters," *IEEE Trans. Ind. Appl.*, vol. 29, no. 2, pp. 313–319, Mar./Apr. 1993.
- [24] M. Ishihara, K. Umetani, H. Umegami, E. Hiraki, and M. Yamamoto, "Quasi-duality between SS and SP topologies of basic electric-field coupling wireless power transfer system," *IET Electron. Lett.*, vol. 52, no. 25, pp. 2057–2059, Dec. 2016.
- [25] W. Zhang and C. C. Mi, "Compensation topologies of high-power wireless power transfer systems," *IEEE Trans. Veh. Technol.*, vol. 65, no. 6, pp. 4768–4778, Jun. 2016.
- [26] K. Umetani, "A generalized method for Lagrangian modeling of power conversion circuit with integrated magnetic components," *IEEE Trans. Elect. Electron. Eng.*, vol. 7, no. S1, pp. S146–S152, Dec. 2012.
- [27] K. Umetani, J. Imaoka, M. Yamamoto, S. Arimura, and T. Hirano, "Evaluation of the Lagrangian method for deriving equivalent circuits of integrated magnetic components: A case study using the integrated winding coupled inductor," *IEEE Trans. Ind. Appl.*, vol. 51, no. 1, pp. 547–555, Jan./Feb. 2015.
- [28] M. Noah, K. Umetani, J. Imaoka, and M. Yamamoto, "Lagrangian dynamics model and practical implementation of an integrated transformer in multi-phase LLC resonant converter," *IET Power Electron.*, vol. 11, no. 2, pp. 339–347, Feb. 2018.
- [29] T. Koyama, T. Honjo, K. Umetani, and E. Hiraki, "Lagrangian derivation and analysis of a simple equivalent circuit model of wireless power transfer system with dual transmitting resonators," in *Proc. Eur. Conf. Power Electron. Appl.*, Karlsruhe, Germany, 2016, pp. 1–10.
- [30] K. Umetani, M. Yamamoto, E. Hiraki, "Lagrangian-based derivation of a novel sliding-mode control for synchronous buck converters," *IEEE Trans. Ind. Appl.*, vol. 4, no. 6, pp. 728–729, Nov. 2015.
- [31] R. Mai, Y. Liu, Y. Li, P. Yue, G. Cao, and Z. He, "An active-rectifier-based maximum efficiency tracking method using an additional measurement coil for wireless power transfer," *IEEE Trans. Power Electron.*, vol. 33, no. 1, pp. 716–728, Jan. 2018.
- [32] W. X. Zhong and S. Y. R. Hui, "Maximum energy efficiency tracking for wireless power transfer systems," *IEEE Trans. Power Electron.*, vol. 30, no. 7, pp. 4025–4034, Jul. 2015.
- [33] R. L. Steigerwald, "A comparison of half-bridge resonant converter topologies," *IEEE Trans. Power Electron.*, vol. 3, no. 2, pp. 174–182, Apr. 1988.



Masataka Ishihara (S'15) received the B.S. and M.S. degrees in electrical engineering from Shimane University, Matsue, Japan, in 2015 and 2017, respectively. He is currently working toward the Ph.D. degree in electrical engineering with the Electric Power Conversion System Engineering Laboratory, Okayama University, Okayama, Japan.

His research interests include wireless power transfer systems, design of integrated magnetic components, and wide bandgap (WBG) power semiconductor device modeling and driving.

Mr. Ishihara is a Member of the Institute of Electrical Engineers of Japan and the Japan Institute of Power Electronics.



Kazuhiro Umetani (M'12) was born in Kobe, Japan. He received the M.S. and Ph.D. degrees in geophysical fluid dynamics from Kyoto University, Kyoto, Japan, in 2004 and 2007, respectively, and the second Ph.D. degree in electrical engineering from Shimane University, Matsue, Japan, in 2015.

From 2007 to 2008, he was a Circuit Design Engineer with Toshiba Corporation, Japan. From 2008 to 2014, he was with the Power Electronics Group, DENSO Corporation, Japan. He is currently an Assistant Professor with the Electric Power Conversion System Engineering Laboratory, Okayama University, Okayama, Japan.

His research interests include new circuit configurations in power electronics and power magnetics for vehicular applications.

Dr. Umetani is a Member of the Institute of Electrical Engineers of Japan and the Japan Institute of Power Electronics.



Eiji Hiraki (M'03) received the M.S. and Ph.D. degrees from Osaka University, Osaka, Japan, in 1990 and 2004, respectively.

In 1990, he joined Mazda Motor Corporation. From 1995 to 2013, he was with the Power Electronics Laboratory, Yamaguchi University, Yamaguchi, Japan. He is currently a Professor with the Electric Power Conversion System Engineering Laboratory, Okayama University, Okayama, Japan. His research interests include circuits and control systems of power electronics, particularly soft-switching technique for high-frequency switching power conversion systems.

Prof. Hiraki is a Member of the Institute of Electrical Engineers of Japan and the Japan Institute of Power Electronics.